Phase transition and structure of silver azide at high pressure

Dongbin Hou, Fuxiang Zhang, Cheng Ji, Trevor Hannon, Hongyang Zhu et al.

Additional information on J. Appl. Phys.

Phase transition and structure of silver azide at high pressure

Dongbin Hou,[1] Fuxiang Zhang,[2] Cheng Ji,[1] Trevor Hannon,[1] Hongyang Zhu,[1] Jianzhe Wu,[1] Valery I. Levitas,[3] and Yanzhang Ma[1,a)]

[1]*Department of Mechanical Engineering, Texas Tech University, Lubbock, Texas 79409, USA*
[2]*Department of Geological Sciences, University of Michigan, Ann Arbor, Michigan 48109-1005, USA*
[3]*Department of Mechanical Engineering, Iowa State University, Ames, Iowa 50011-2161, USA*

Silver azide (AgN_3) was compressed up to 51.3 GPa. The results reveal a reversible second-order orthorhombic-to-tetragonal phase transformation starting from ambient pressure and completing at 2.7 GPa. The phase transition is accompanied by a proximity of cell parameters a and b, a 3° rotation of azide anions, and a change of coordination number from 4-4 (four short, four long) to eight fold. The crystal structure of the high pressure phase is determined to be in $I4/mcm$ space group, with Ag at $4a$, N_1 at $4d$, and N_2 at $8h$ Wyckoff positions. Both of the two phases have anisotropic compressibility: the orthorhombic phase exhibits an anomalous expansion under compression along a-axis and is more compressive along b-axis than c-axis; the tetragonal phase is more compressive along the interlayer direction than the intralayer directions. The bulk moduli of the orthorhombic and tetragonal phases are determined to be $K_{OT} = 39 \pm 5$ GPa with $K_{OT}' = 10 \pm 7$ and $K_{OT} = 57 \pm 2$ GPa with $K_{OT}' = 6.6 \pm 0.2$, respectively. © *2011 American Institute of Physics*. [doi:10.1063/1.3610501]

I. INTRODUCTION

Inorganic azides have attracted considerable attention[1–3] due to their application in energetic explosives and gas generators.[4–10] The innocuous properties of the product gases make them a green energy source that may decrease the greenhouse effect.[11] Furthermore, their theoretical importance as simple systems modeling the interatomic forces makes them applicable to study for both the structure and the dynamics in various phases under different pressure or temperature conditions.[12–14]

Metal azides undergo a variety of pressure or temperature-induced phase transitions, a phenomenon which has been intensively studied.[14–25] The behavior of the azide anions (N_3^-) during the phase transition is noticeable. In the temperature-induced tetragonal-cubic phase transitions of both rubidium azide (RbN_3) and cesium azide (CsN_3), a fluctuation of the orientation of N_3^- anions was observed.[16–18] In both the temperature-[15] and pressure-induced[23–25] rhombohedral-monoclinic phase transition of sodium azide (NaN_3), a tilting of N_3^- anions was also observed. High-pressure studies on metal azides are of special interest recently because of their use as a precursor to form a highly energetic polymeric (non-molecular) form of nitrogen (N_2). From years of studies of N_2, a polymeric N_2 phase under high pressure was first predicted in 1985 (Ref. 26) and later investigated by optical and electrical methods in 2000 (Ref. 27) and 2001,[28] respectively. A single-bonded cubic gauche form of N_2 was successfully synthesized in 2004 (Ref. 29) and 2007.[30] Simultaneously, the N_3^- anions in NaN_3 were also found to transform to polymeric nitrogen nets under high pressure in 2004 (Ref. 19) and a cubic gauche structure in 2005.[20] A high-pressure study on lithium azide (LiN_3) also pre-

dicted the formation of a polymeric nitrogen network with further compression beyond its pressure range studied.[31] The mechanism of photolysis of NaN_3 under high pressure was also studied to help elucidate the potential for high-pressure syntheses of novel nitrogen structures.[32] In this respect, a study of the high-pressure behavior of AgN_3 would provide more insight into the mechanism of pressure-induced rearrangement of N_3^- anions and phase transitions that might result in the formation of polymeric nitrogen.

AgN_3 has been studied intensively due to its high efficiency as a detonating agent for explosives and gas generator.[7–10] Its crystal structure has been the subject of several investigations.[33–37] Under ambient conditions, AgN_3 crystallizes in orthorhombic space group *Ibam* (Fig. 1), with $a = 5.600(1)$, $b = 5.980(6)$, $c = 5.998(1)$ Å, and $Z = 4$.[37] Upon heating from room temperature, its a-axis shows an anomalous behavior, since it shrinks with temperature.[38] AgN_3 exhibits an irreversible temperature-induced phase transition at 170 °C to a monoclinic structure in $P2_1/c$ space group.[38] Despite the considerable previous studies on AgN_3, no study on its high pressure structure has been reported yet. Comparing to its high temperature behavior, the possible phase transition and anomalous behavior of a-axis under high pressure are also interesting to be investigated.

The present paper reports the pressure-induced phase transformation and compressibility of AgN_3 by means of a synchrotron X-ray diffraction measurement to 51.3 GPa in a diamond anvil cell.

II. EXPERIMENT

A symmetric diamond anvil cell with flat diamonds was used to generate high pressure in the experiments. The anvil was 400 μm in diameter. A rhenium gasket was used, with a hole of 150 μm in diameter and 60 μm in thickness, as the

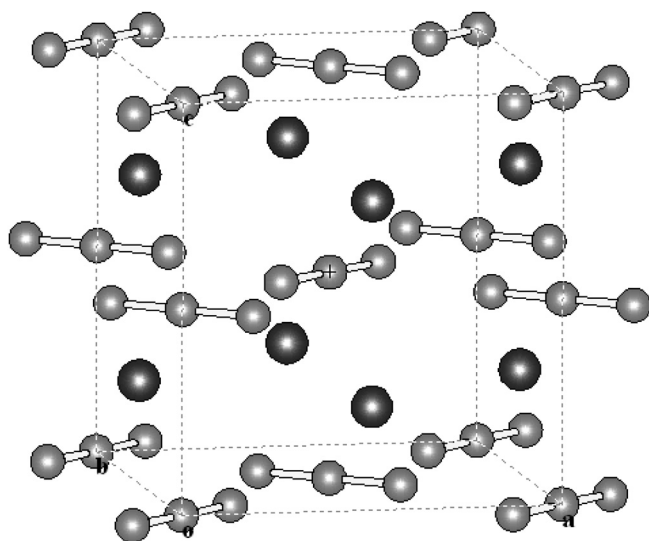a)Author to whom correspondence should be addressed. Electronic mail: y.ma@ttu.edu.

FIG. 1. The crystal structure of ambient AgN_3. The Ag atoms are represented by black spheres and N atoms by gray spheres.

sample chamber. AgN_3 was prepared by mixing equimolar amounts of aqueous solutions of NaN_3 and $AgNO_3$ at room temperature and washing the as-received white precipitate several times with de-ionized water.[39] The sample was dried at ambient conditions for 12 h. Finally, the sample was stored in the dark due to the light sensitivity of this compound. A small flake of the sample with ~100 μm in diameter and ~30 μm in thickness was loaded into the sample chamber. Pressure was measured by the nonlinear shift of the wavelength of the ruby R1 line.[40,41] Argon gas and a methanol-ethanol mixture in a 4:1 volume ratio were selected as pressure transmitting media in different experimental runs to rule out the possible contamination by products of the reaction of AgN_3 with the pressure media. *In situ* high-pressure angle-dispersive X-ray diffraction experiments at room temperature were performed at the beamline B2 of the Cornell High Energy Synchrotron Source (CHESS, Wilson Laboratory) at Cornell University and the beamline X17 C in the National Synchrotron Light Source (NSLS) at Broo-

FIG. 2. X-ray diffraction patterns of AgN_3 at selected pressures.

khaven National Laboratory. In CHESS, the X-ray had a wavelength of 0.4859 Å and was collimated to a beam size of 40 μm in diameter; the diffraction data were recorded on a MAR345 imaging plate. In NSLS, the X-ray beam had a wavelength of 0.4066 Å and was focused to a spot size of 30×30 μm^2; the diffraction data were collected using a MAR CCD detector. The diffraction images were converted to 2θ versus intensity data plots using the FIT2 D software.[42] The diffraction patterns were analyzed by the software package of FullProf.[43]

III. RESULTS AND DISCUSSION

The AgN_3 sample was compressed up to 51.3 GPa. The results reveal a second-order phase transformation, starting from ambient pressure and completing at 2.7 GPa. The ambient phase was recovered upon decompression to the ambient condition. Representative patterns are shown in Fig. 2.

At ambient condition, 33 peaks were resolved and indexed to the orthorhombic structure with *Ibam* symmetry (Phase II). The cell parameters obtained at ambient condition, $a = 5.602(2)$, $b = 5.938(2)$, and $c = 6.022(1)$, are in excellent agreement with the results in the literature.[37] Under compression, the b and c axes shrink, while the a-axis shows an anomalous behavior, since it expands with increasing pressure. Meanwhile, b-axis shrinks significantly under compression, which leads to a proximity of the length of a and b ($b > a$ at ambient condition) until an equality of $a = b$ is satisfied at 2.7 GPa. As a result, a phase transition from orthorhombic to tetragonal structure is induced. The change of cell parameters are tabulated in Table I and illustrated in Fig. 3, which will be further discussed in the following texts. The process of the transition can also be explicitly observed in the diffraction patterns (Fig. 2). It is clearly shown that the (200) peak shift toward high d-spacing angle until 1.0 GPa, which shows the expansion of a under compression. The proximity of a and b can be clearly observed by the proximity of (020) and (200), (022) and (202), and (130) and (310) peaks up to 2.7 GPa (indicated by the dashed lines in Fig. 2). From the process of the transition, it can be concluded that it is a continuous, second-order phase transition[44] induced by an addition of $a = b$ symmetry in the unit cell. This will also be confirmed in the following text.

The structure of the high pressure phase of AgN_3 (HP-AgN_3) at 2.7 GPa was indexed by DICVOL, and the result is illustrated in Fig. 4. By comparing the indices before and after the phase transition, an excellent agreement is shown between the two phases: all the peaks of HP-AgN_3 have identical indices as the ambient phase; the only difference is that the peaks of (020), (022), and (130) in ambient phase merged into (200), (202), and (310) peaks in HP-AgN_3, respectively. This double confirms that the phase transition is a continuous, second-order transition induced by an addition of $a = b$ symmetry. By checking the systematic extinctions, three of them were observed: (hhl) with l odd, (0kl) with k or l odd, (hkl) with $h + k + l$ odd. They lead to three possible space groups of HP-AgN_3: $I4/mcm$, $I4cm$, and $I\bar{4}c2$. The $I4/mcm$ belongs to the centrosymmetric point group $4/mmm$; $I4cm$ and $I\bar{4}c2$ belong to the non-centrosymmetric
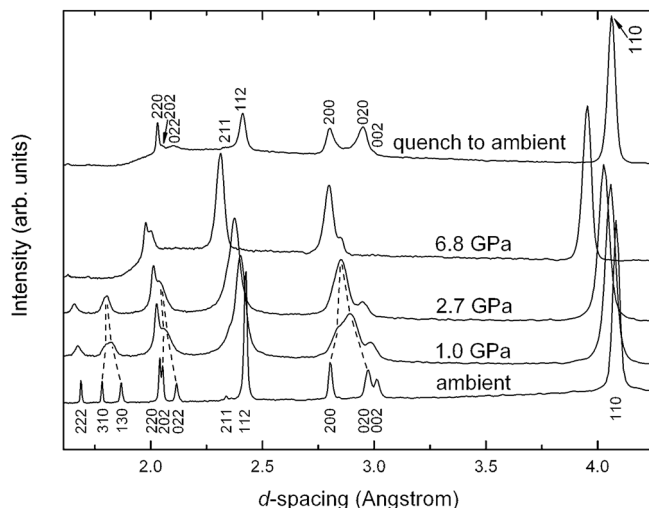
TABLE I. Unit cell parameters and unit cell volume of AgN$_3$ at varying pressures. The signs of "(ME)" and "(A)" after the pressure values indicate the measurements were taken using the pressure media of methanol-ethanol mixture in a 4:1 volume ratio and argon gas, respectively. The signs of "d:" before the pressure values indicate the measurements were taken in the decompression process. The numbers in the parentheses represent the error in the last digit resulted from the refinement.

Pressure (GPa)	a (Å)	b (Å)	c (Å)	V (Å^3)
Ambient	5.602(2)	5.938(2)	6.022(1)	200.3(1)
0.2(ME)	5.617(6)	5.909(6)	6.020(3)	199.8(3)
0.3(ME)	5.626(8)	5.900(7)	6.019(4)	199.8(4)
0.5(ME)	5.644(9)	5.856(8)	5.995(5)	198.1(4)
0.7(ME)	5.657(9)	5.827(9)	5.976(5)	197.0(5)
1.0(ME)	5.66(1)	5.80(1)	5.957(5)	195.6(5)
1.2(ME)	5.66(1)	5.79(1)	5.952(6)	195.3(5)
1.5(ME)	5.66(1)	5.77(1)	5.935(6)	194.1(5)
1.7(ME)	5.66(1)	5.76(1)	5.921(6)	193.1(5)
2.0(ME)	5.65(1)	5.74(1)	5.901(5)	191.7(5)
2.3(ME)	5.65(1)	5.73(1)	5.890(6)	191.0(5)
2.7(ME)	5.689(8)		5.874(5)	190.1(4)
3.3(A)	5.65(1)		5.798(8)	185.1(7)
3.9(A)	5.63(1)		5.773(7)	183.3(6)
4.5(A)	5.62(1)		5.754(8)	181.9(7)
5.2(ME)	5.618(2)		5.742(1)	181.24(9)
6.0(A)	5.60(2)		5.714(9)	179.3(8)
6.8(A)	5.60(1)		5.703(7)	178.7(6)
7.0(ME)	5.592(2)		5.696(1)	178.1(1)
9.4(ME)	5.556(2)		5.635(1)	173.9(1)
12.2(A)	5.54(2)		5.60(1)	171.7(8)
13.8(A)	5.52(2)		5.57(1)	169.8(9)
15.0(A)	5.51(2)		5.55(1)	168.4(9)
15.7(A)	5.50(1)		5.539(8)	167.3(7)
17.6(A)	5.47(2)		5.51(1)	165(1)
19.2(A)	5.44(2)		5.48(1)	162(1)
21.6(A)	5.42(3)		5.45(1)	160(1)
24.6(A)	5.39(3)		5.41(1)	157(1)
29.3(A)	5.37(4)		5.35(2)	154(2)
31.4(A)	5.34(1)		5.323(6)	151.7(5)
44.3(ME)	5.280(9)		5.218(7)	145.5(4)
46.7(ME)	5.267(9)		5.202(7)	144.3(4)
51.3(ME)	5.238(8)		5.155(6)	141.4(4)
d: 16.2(A)	5.46(4)		5.49(2)	164(2)
d: 15.4(A)	5.47(4)		5.50(2)	164(2)
d: 15.1(A)	5.48(4)		5.50(2)	165(2)
d: 14.0(A)	5.48(4)		5.52(2)	166(2)
d: 11.6(A)	5.52(3)		5.56(2)	169(1)
d: 9.2(A)	5.54(3)		5.60(2)	172(1)
d: 8.1(A)	5.57(3)		5.63(2)	174(1)
d: 7.1(A)	5.57(2)		5.65(2)	175(1)
d: 3.0(A)	5.65(2)		5.80(2)	185(1)
Quench to ambient	5.61(2)	5.88(1)	5.99(1)	197.5(8)

FIG. 3. The pressure dependence of the cell parameters *a*, *b*, and *c* of AgN$_3$.

assigned as *I4/mcm*. To assign the Wyckoff positions for each atom in HP-AgN$_3$, it is found that, among all the known structures of metal azides, to our knowledge, there exist only four compounds crystallizing in the space group of *I4/mcm* (which are the ambient phases of potassium azide, rubidium azide, cesium azide, and thallous azide[45,46]), and all of them possess the same Wyckoff positions as: metal at *4a*, N$_1$ at *4d*, and N$_2$ at *8h*. Furthermore, it is also found that these Wyckoff positions are closely analogous to that of ambient AgN$_3$. Therefore, the Wyckoff positions of HP-AgN$_3$ atoms are assigned as: Ag at *4a*, N$_1$ at *4d*, and N$_2$ at *8h* (these positions result in a Z number of 4, which is also consistent with the ambient AgN$_3$ structure).

To investigate the atomic coordinates of HP-AgN$_3$, the diffraction patterns were refined by Rietveld method. The best refinement of our experimental data was achieved when fitting the data of argon gas as the pressure medium in the pressure range from 13.8 to 31.4 GPa. We believe this is because argon gas has a better performance in this pressure range. Figure 5 shows the Rietveld plot at 13.8 GPa. The

point groups 4*mm* and $\overline{4}2m$, respectively. The space group of ambient AgN$_3$ is *Ibam*, which belongs to the centrosymmetric point group *mmm*. Because the phase transition is a continuous, second-order transition induced by an addition of *a = b* symmetry, it can be inferred that the inversion symmetry element is preserved during the phase transition; in consequence, the point group is changed from centrosymmetric *mmm* to centrosymmetric 4/*mmm* by an addition of the symmetric element of fourfold axis parallel to *c*-axis. Therefore, the space group of HP-AgN$_3$ is
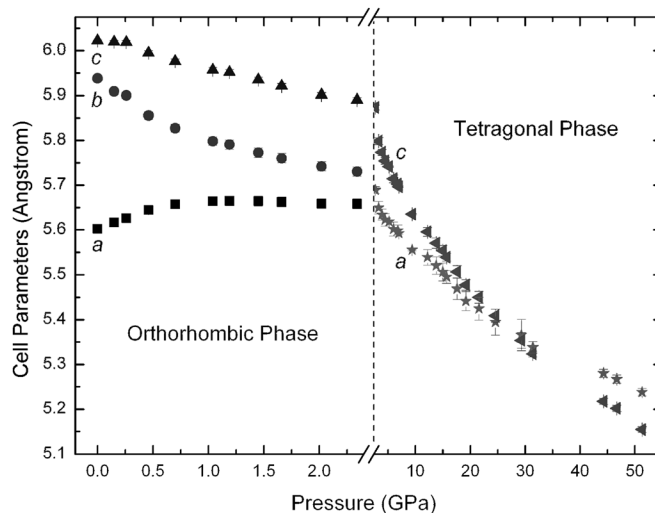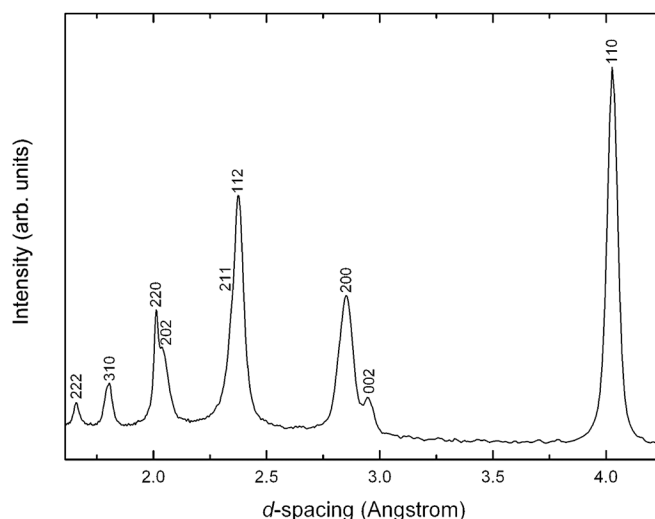
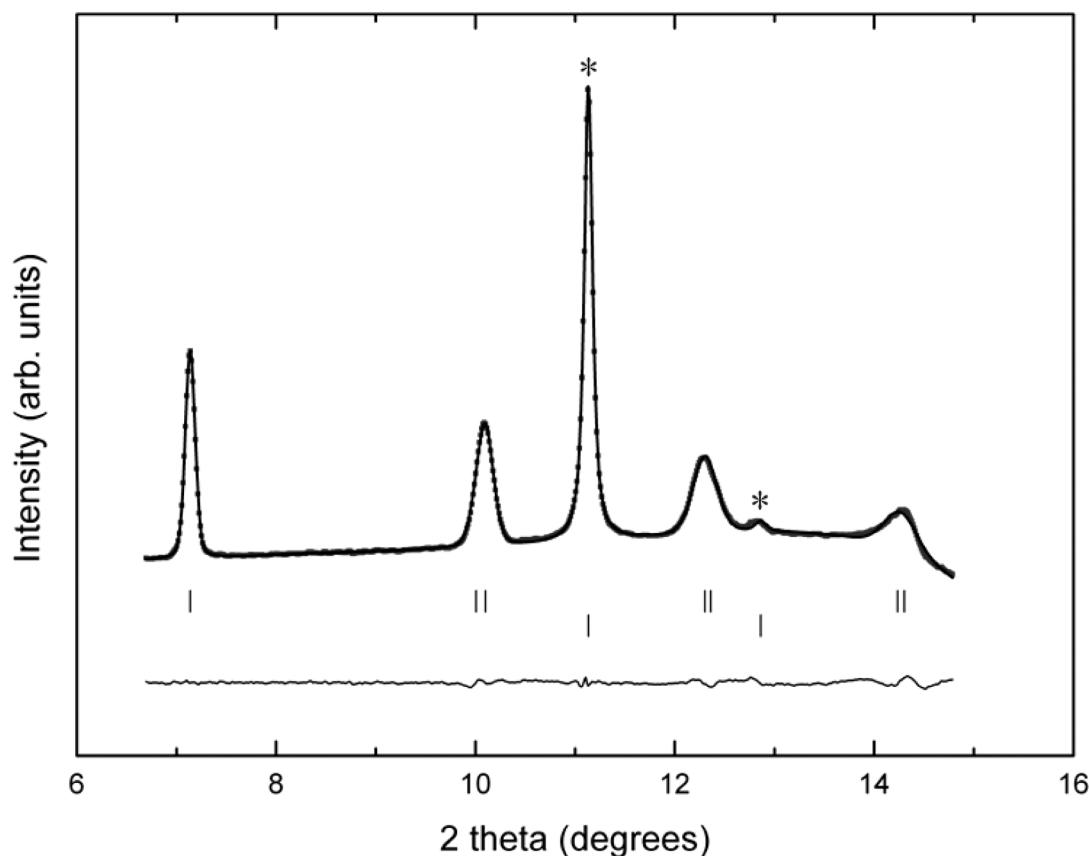

FIG. 4. The miller indices of HP-AgN$_3$ at 2.7 GPa.

FIG. 5. Rietveld refinement patterns for HP-AgN$_3$ at 13.8 GPa. The observed diffraction intensities are represented by the dots and the calculated pattern by the bold solid line. The solid curve at the bottom represents the difference between the observed and calculated intensities. Short vertical bars below the observed and calculated patterns indicate the positions of allowed Bragg reflections. The asterisks "*" indicate the peaks from the pressure transmitting medium argon. The wavelength of X-ray is 0.4859 Å.

mean quality factors of the refinement are $R_p = 0.871\%$, $R_{wp} = 1.18\%$, and $\chi^2 = 0.00514$. It is shown that the calculated curve fits the experimental data reasonably well, indicating a correct assignment of space group and Wyckoff positions. The resulting atomic fractional coordinates are summarized in Table II and plotted in Fig. 6. The results indicate that the change in going from the orthorhombic to the tetragonal phase is from 4-4 coordination (four short, four long) to eight fold coordination of the Ag. Each azide anion has undergone a small rotation of 3° about an axis through the central nitrogen atom and normal to the *ab* plane to an orientation inclined at an angle of 45° to the *ac* (or *bc*) plane. It should be pointed out that the large difference in the scattering ability of Ag and N may result in a larger error in the atomic fractional coordinates of N$_2$ than those shown in the fitting results.

As shown in Table I and Fig. 3, the compressibility of orthorhombic AgN$_3$ shows considerable anisotropy. The anomalous behavior (expansion) of *a* at high pressure is in accord with its anomalous behavior (shrink) at high temperature.[38] It may contribute to the detonation of AgN$_3$ on mechanical impact, where the necessary internal stress could result from the anomalous behavior of the lattice parameter *a* of orthorhombic AgN$_3$.[38] The deformation of *b* is higher than of *c* (*b* shrinks 4% from ambient pressure to 2.3 GPa; while *c* shrinks 2%) at high pressure, which is also in accord

with the higher deformation of *b* than of *c* at high temperature.[38] Because of the remarkable consistence in the cell parameters' behavior of orthorhombic AgN$_3$ at both high pressure and high temperature,[38] it is reasonable to infer that the orthorhombic-to-tetragonal phase transition is favored by low temperature as well. Linear fitting the P-V data of the orthorhombic phase (Table I) yields a shrink coefficient of −4.0 (1) Å^{3}GPa^{-1} at high pressure; comparing this value with its linear thermal expansion coefficient of 0.0365 Å^{3}K^{-1} at high temperature,[38] roughly one can equate the effect of a rise of 1 GPa in pressure to a drop of 110 °C in temperature. The compressibility of HP-AgN$_3$ is also anisotropic, with *c*-axis more compressive than *a*-axis. Since HP-AgN$_3$ has a layered structure of alternating Ag cation and azide anion layers (as seen in Fig. 6), its anisotropic compressibility indicates that it is more compressive along interlayer direction than intralayer directions. This can be ascribed to the attraction force between the cation and anion ions and the repulsion force between the same type of (either cation or anion) ions.

The unit cell volume of AgN$_3$ at varying pressures is summarized in Table I. The unit cell volume changes continuously with only an inflection at the transition, which further confirms that the transition is a continuous, second-order phase transition. To determine the bulk modulus K$_{OT}$ and its pressure derivative K$_{OT}$', the Birch–Murnaghan Equation of State (BM EOS)[47] was applied,

TABLE II. Atomic fractional coordinates of HP-AgN$_3$ at 13.8 GPa. The Wyck stands for the Wyckoff positions of space group $I4/mcm$. The numbers in the parentheses represent the error in the last digit resulted from the refinement.

Atom	Wyck	x	y	z
Ag	4a	0	0	0.25
N$_1$	4d	0	0.5	0
N$_2$	8h	0.16(2)	0.66(2)	0

$$P = \frac{3}{2} K_{OT} \left[\left(\frac{V_0}{V} \right)^{7/3} - \left(\frac{V_0}{V} \right)^{5/3} \right] \left\{ 1 + \frac{3}{4}(K' - 4) \left[\left(\frac{V_0}{V} \right)^{2/3} - 1 \right] \right\},$$

where V_0 is the volume at ambient pressure, K_{OT} is the bulk modulus at ambient pressure and temperature, and K_{OT}' is the pressure derivative of K_{OT}. A least-squares fitting of pressure-volume data to the BM EOS was performed. A systematic pressure error of 0.1 GPa and random volume errors from the volume refinement were used in the analysis. Fitting the data to the third-order BM EOS yields a bulk modulus of $K_{OT} = 39 \pm 5$ GPa with its pressure derivative of $K_{OT}' = 10 \pm 7$ for the low pressure orthorhombic phase and $K_{OT} = 57 \pm 2$ GPa with $K_{OT}' = 6.6 \pm 0.2$ for the high pressure tetragonal phase. By calculating the volume of HP-AgN$_3$ at 2.7 GPa using the BM EOS, the volume reduction at the phase transition is found to be 1%. The unit cell volume as a function of pressure is shown in Fig. 7, in which the solid lines demonstrate the fitting curve using the third-order BM EOS. Comparing the bulk modulus of AgN$_3$ with LiN$_3$ ($K_{OT} = 19.1 \pm 1.4$ GPa with $K_{OT}' = 7.3 \pm 0.5$),[31] it is found that AgN$_3$ is much less compressible than LiN$_3$. This can be ascribed to the ionic character of the Li-azide bond and the covalent character of the Ag-azide bond.[46]
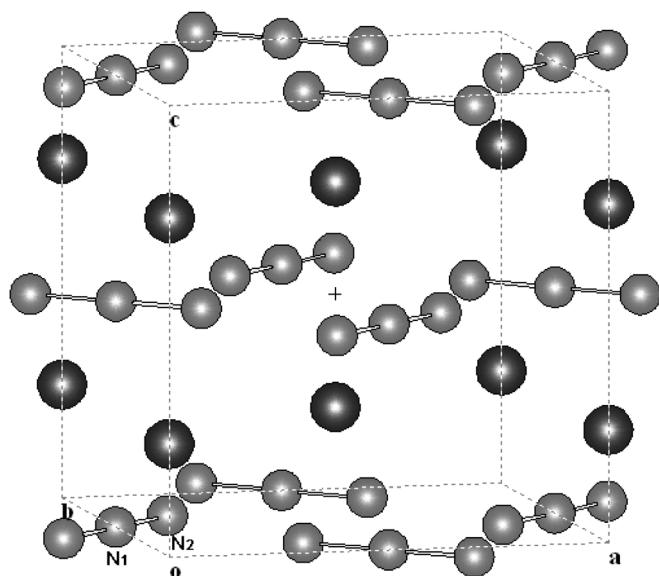

FIG. 6. The crystal structure of HP-AgN$_3$ yielded from the refinement at 13.8 GPa. The Ag atoms are represented by black spheres and N atoms by gray spheres.
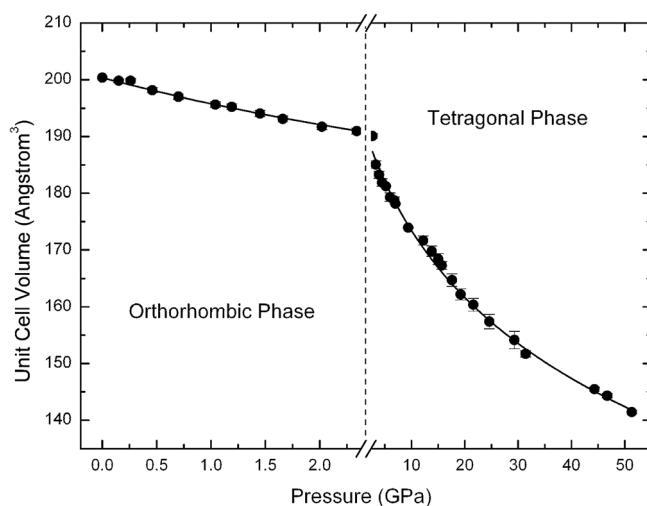

FIG. 7. The change of AgN$_3$ unit cell volume with pressure. The solid lines demonstrate the fitting of the P-V data to the third-order Birch-Murnaghan equation of state.

It is of note that the orthorhombic-to-tetragonal phase transition of AgN$_3$ at high pressure is closely analogous to the tetragonal-to-orthorhombic transition of TlN$_3$ at low temperature,[46] based on the facts that both of them possess: 1) the anomalous behavior of the orthorhombic phase, 2) the same Wyckoff positions of the tetragonal phase, and 3) the continuous volume change during phase transition. This may imply that the low temperature orthorhombic phase of TlN$_3$ might be isostructural with orthorhombic AgN$_3$.

IV. CONCLUSIONS

High-pressure study of AgN$_3$ up to 51.3 GPa revealed a reversible second-order orthorhombic-to-tetragonal phase transformation, starting from ambient pressure and completing at 2.7 GPa. The phase transition is accompanied by a proximity of cell parameters a and b, a 3° rotation of azide anions, and a change of coordination number from 4-4 (four short, four long) to eight fold. The high pressure phase is in the space group of $I4/mcm$, with Wyckoff positions of $4a$ (Ag), $4d$ (N$_1$), and $8h$ (N$_2$). The lattice parameter a of the orthorhombic phase exhibits an anomalous expansion under compression. Of the orthorhombic phase, the lattice parameter b is more compressive than c, and, of the tetragonal phase, c (along interlayer direction) is more compressive than a (along intralayer direction). The bulk moduli of the orthorhombic and tetragonal phases are determined to be $K_{OT} = 39 \pm 5$ GPa with $K_{OT}' = 10 \pm 7$ and $K_{OT} = 57 \pm 2$ GPa with $K_{OT}' = 6.6 \pm 0.2$, respectively.

[1] B. L. Evans and A. D. Yoffe, Proc. R. Soc. London, Ser. A **238**, 568 (1957).
[2] B. L. Evans, A. D. Yoffe, and P. Gray, Chem. Rev. (Washington, D. C.) **59**, 515 (1959).
[3] I. Agrell, Acta Chem. Scand. **25**, 2965 (1971).

[4]C. M. Pereira and M. M. Chaudhri, J. Energ. Mater. **7**, 297 (1989).

[5]B. P. Aduev, E. D. Aluker, G. M. Belokurov, Y. A. Zakharov, and A. G. Krechetov, J. Exp. Theor. Phys. **89**, 906 (1999).

[6]S. K. Deb, B. L. Evans, and A. D. Yoffe, Sym. (Int.) Combust. [Proc.] **8**, 829 (1962).

[7]T. B. Tang and M. M. Chaudhri, Proc. R. Soc. London, Ser. A **369**, 83 (1979).

[8]A. C. McLaren and G. T. Rogers, Proc. R. Soc. London, Ser. A **240**, 484 (1957).

[9]F. P. Bowden and A. C. McLaren, Proc. R. Soc. London, Ser. A **246**, 197 (1958).

[10]M. M. Chaudhri, Nature (London), Phys. Sci. **242**, 110 (1973).

[11]A. Midilli, I. Dincer, and M. Ay, Energy Policy **34**, 3623 (2006).

[12]C. E. Weir, S. Block, and G. J. Piermarini, J. Chem. Phys. **53**, 4265 (1970).

[13]J. Liu, C. G. Duan, M. M. Ossowski, W. N. Mei, R. W. Smith, and J. R. Hardy, Mater. Res. Bull. **36**, 2035 (2001).

[14]C. W. F. T. Pistorius, J. Chem. Phys. **51**, 2604 (1969).

[15]G. E. Pringle and D. E. Noakes, Acta Crystallogr., Sect. B: Struct. Crystallogr. Cryst. Chem. **24**, 262 (1968).

[16]H. J. Mueller and J. A. Joebstl, Z. Kristallogr. **121**, 385 (1965).

[17]Z. Iqbal and C. W. Christoe, J. Chem. Phys. **62**, 3246 (1975).

[18]F. J. Owens, J. Phys. C **12**, 2255 (1979).

[19]M. I. Eremets, M. Y. Popov, I. A. Trojan, V. N. Denisov, R. Boehler, and R. J. Hemley, J. Chem. Phys. **120**, 10618 (2004).

[20]M. Popov, Phys. Lett. A **334**, 317 (2005).

[21]Z. Iqbal and C. W. Christoe, Solid State Commun. **17**, 71 (1975).

[22]S. R. Aghdaee and A. I. M. Rae, Acta Crystallogr., Sect. B: Struct. Sci. **B 40**, 214 (1984).

[23]G. J. Simonis and C. E. Hathaway, Phys. Rev. B **10**, 4419 (1974).

[24]L. B. Kanney, N. S. Gillis, and J. C. Raich, J. Chem. Phys. **67**, 81 (1977).

[25]Z. Iqbal, J. Chem. Phys. **59**, 1769 (1973).

[26]A. K. McMahan and R. LeSar, Phys. Rev. Lett. **54**, 1929 (1985).

[27]A. F. Goncharov, E. Gregoryanz, H.-k. Mao, Z. Liu, and R. J. Hemley, Phys. Rev. Lett. **85**, 1262 (2000).

[28]M. I. Eremets, R. J. Hemley, H.-k. Mao, and E. Gregoryanz, Nature **411**, 170 (2001).

[29]M. I. Eremets, A. G. Gavriliuk, I. A. Trojan, D. A. Dzivenko, and R. Boehler, Nature Mater. **3**, 558 (2004).

[30]M. I. Eremets, A. G. Gavriliuk, and I. A. Trojan, Appl. Phys. Lett. **90**, 171904 (2007).

[31]S. A. Medvedev, I. A. Trojan, M. I. Eremets, T. Palasyuk, T. M. Klapoetke, and J. Evers, J. Phys.: Condens. Matter **21**, 195404 (2009).

[32]S. M. Peiris and T. P. Russell, J. Phys. Chem. A **107**, 944 (2003).

[33]M. Bassiere, Compt. Rend. **201**, 735 (1935).

[34]C. D. West, Z. Kristallogr. **95**, 421 (1936).

[35]E. W. Hughes, Doctoral thesis, Cornell University, 1935.

[36]H. G. Pfesiffer, Doctoral thesis, California Institute of Technology, 1948.

[37]G.-C. Guo, Q.-M. Wang, and T. C. W. Mak, J. Chem. Cryst. **29**, 561 (1999).

[38]C. L. Schmidt, R. Dinnebier, U. Wedig, and M. Jansen, Inorg. Chem. **46**, 907 (2007).

[39]R. L. Brooks, Mater. Res. Bull. **3**, 389 (1968).

[40]H. K. Mao, P. M. Bell, J. W. Shaner, and D. J. Steinberg, J. Appl. Phys. **49**, 3276 (1978).

[41]H. K. Mao, J. Xu, and P. M. Bell, J. Geophys. Res. B **91**, 4673 (1986).

[42]A. P. Hammersley, S. O. Svensson, M. Hanfland, A. N. Fitch, and D. Hausermann, High Press. Res. **14**, 235 (1996).

[43]J. Rodriguez-Carvajal, Physica B **192**, 55 (1993).

[44]M. T. Dove, Am. Mineral. **82**, 213 (1997).

[45]W. Zhu, J. Xiao, and H. Xiao, J. Phys. Chem. B **110**, 9856 (2006).

[46]F. A. Mauer, C. R. Hubbard, and T. A. Hahn, J. Chem. Phys. **59**, 3770 (1973).

[47]F. Birch, Phys. Rev. **71**, 809 (1947).